Optical Properties of $Cd_{0.9}Zn_{0.1}Te$ Studied by Variable Angle Spectroscopic Ellipsometry between 0.75 and 6.24 eV

H.W. Yao [a),b)], J.C. Erickson [a),b)], H.B. Barber [c)], R.B. James [b)], and H. Hermon [b)]

a) University of Nebraska, Lincoln, NE 68588; hyao@unl.edu;
b) Sandia National Laboratories, Livermore, CA 94551;
c) University of Arizona, Tucson, AZ 85724;

ABSTRACT

Optical properties of $Cd_{0.9}Zn_{0.1}Te$ (CZT) were studied by variable angle spectroscopic ellipsometry (VASE). Measurements made by VASE were performed on CZT and CdTe samples in air at room temperature at multiple angles of incidence. A parametric function model was employed in the VASE analysis to determine the dielectric functions $\varepsilon = \varepsilon_1 + i\varepsilon_2$ in the range of 0.75 to 6.24 eV. A two-oscillator analytical model was used to describe the dielectric response of native oxides on CZT. Surface oxide optical properties and thickness on CZT were also determined in conjunction with the VASE measurement and analysis of a CdTe sample. Two samples of CZT of different oxide thicknesses were measured and their optical constants were coupled together in a multiple-sample, multiple-model VASE analysis to resolve correlations between fitting parameters. Effective medium approximation (EMA) was used to describe the optical properties of the CZT oxide with roughness. A Kramers-Kronig self-consistency check of the real and imaginary parts of the $Cd_{0.9}Zn_{0.1}Te$ dielectric functions was performed over the energy range 0.75 to 6.24 eV. A five-Lorentz-oscillator model was employed to describe the dielectric response of CZT in the range of 1.6 to 6.24 eV. Intensity

transmission measurements were made on the $Cd_{0.9}Zn_{0.1}Te$ and CdTe, showing the absorption energy band edges of ~1.58 and 1.46 eV, respectively.

1. Introduction

Cadmium Zinc Telluride (CZT) is a leading technological material for room-temperature gamma-ray and x-ray detectors. CZT also has great potential for widespread commercial use in such applications as medical imaging, environmental monitoring, and possibly remote sensing x-ray and gamma-ray spectrometers. CZT's energy resolution, efficiency, and low bias voltage requirement are driving the material growth industry to produce larger detector grade crystals at reasonable cost.[1]

The optical properties of CZT crystal is an important part of characterizing detector performance by accurately predicting response due to changes in alloy fraction or crystal growth methods as well as evaluating crystals grown using new techniques. However, the optical dielectric response of the CZT crystal, e.g., dielectric functions $\varepsilon = \varepsilon_1 + i\varepsilon_2$, as well as optical properties of native oxide on CZT have not been determined by precise optical measurements. In this paper, we report determination of room temperature dielectric functions of $Cd_{0.9}Zn_{0.1}Te$ crystal in a spectral range of 0.75 to 6.24 eV, by variable angle spectroscopic ellipsometry (VASE). The optical properties of native oxide on CZT were estimated through evaluations of the dielectric reponse of oxide on CdTe using a two-oscillator analytical model. A parametric model in a multiple-sample, multiple-model VASE analysis was then used to describe the dielectric function for $Cd_{0.9}Zn_{0.1}Te$ in conjunction with effective medium approximation (EMA) implemented to describe the rough oxidized CZT surface. A Kramers-Kronig self-consistency

DISCLAIMER

DISCLAIMER

Portions of this document may be illegible in electronic image products. Images are produced from the best available original document.

check was performed to ensure that the resulting dielectric function is correctly correlated. A five-Lorentz-oscillator model is implemented to analytically describe the dielectric function for $Cd_{0.9}Zn_{0.1}Te$. Transmission intensity measurements are presented for both CdTe and $Cd_{0.9}Zn_{0.1}Te$ to demonstrate the difference in energy-band absorption edges between the two materials.

2. Ellipsometry Background

Spectroscopic ellipsometry is a non-invasive optical technique sensitive to fractions of atom layer thickness, capable of determining surface changes, optical constants of bulk or layered materials, overlayer thickness, multi-layer structures, and surface or interface roughness.[2-4] The measured ellipsometry parameters ψ and Δ are related to the complex ratio of reflection coefficients r_p and r_s where the angle of incident light is given by ϕ. Here the subscripts 'p' and 's' refer to light polarized parallel (p) and perpendicular (s) to the plane of incidence.[3] The ratio is defined as

$$\rho = \frac{r_p}{r_s}\tan(\psi)e^{i\Delta} \tag{1}$$

The parameters ψ and Δ are sensitive to changes in surface conditions, overlayer thickness, dielectric functions and other properties of the sample.[2,3,5] The measured ellipsometric parameters ψ and Δ are related to the pseudodielectric function given by

$$\langle\varepsilon\rangle = \langle\varepsilon_1\rangle + i\langle\varepsilon_2\rangle = \sin^2\phi\left[1+\tan^2\phi\left(\frac{1-\rho}{1+\rho}\right)^2\right] \tag{2}$$

For a simple sample with no overlayer ρ could be used to determine the dielectric response directly using Eq. 2. However, the substrate in general is covered with a surface overlayer, i.e.,

native oxide layer, surface roughness, etc. In this case, we must numerically fit the ellipsometric data to an assumed model through a regression analysis. During this regression the differences between the calculated and experimental values are minimized, via a mean squared error (MSE) function. The MSE is defined as

$$MSE = \frac{1}{2N-M}\sum_{i=1}^{N}\left[\left(\frac{\psi_i^{\mathrm{mod}}-\psi_i^{\mathrm{exp}}}{\sigma_{\psi,i}^{\mathrm{exp}}}\right)^2+\left(\frac{\Delta_i^{\mathrm{mod}}-\Delta_i^{\mathrm{exp}}}{\sigma_{\Delta,i}^{\mathrm{exp}}}\right)^2\right]=\frac{1}{2N-M}\chi^2 \qquad (3)$$

where N is the number of (ψ, Δ) pairs, M is the number of variable parameters in the model, and σ are the standard deviations on the experimental data points.

3. Experimental

Multiple angle spectroscopic ellipsometric measurements of two $Cd_{0.9}Zn_{0.1}Te$ and one CdTe samples were made in the spectral range of 0.75 to 6.24 eV (0.75 to 5.5 for one CZT sample) with an increment of 0.02 eV, at angles of incidence of 73°, 75°, and 77°. Transmission intensity measurements of CZT and CdTe were taken in the range 0.75 eV to 3.5 eV with an increment of 0.02 eV. The ellipsometry measurements were acquired using a variable angle spectroscopic ellipsometer (VASE), equipped with a beam-chopped, rotating-analyzer to increase stray light rejection and signal to noise ratio, and an auto-retarder for more accurate measurements of ψ and Δ at 0°. Both $Cd_{0.9}Zn_{0.1}Te$ samples (samples A and B) were grown using a vertical high-pressure Bridgman method. Sample A was well polished on both surfaces while sample B was only one surface polished. Transmission intensity measurements could only be acquired on sample A since the measurement requires two parallel polished surfaces.

4. Results and Data Analysis

To obtain the optical constants of the CZT substrate covered by the native oxide layer, an assumed surface model and regression analysis of the spectroscopic ellipsometry data are needed. The optical constants of native oxide needed for modeling is unknown. As an alternative, dielectric optical response of native oxide on CdTe was measured by VASE and applied to the CZT surface model calculation as initial value. The optical dielectric functions of $Cd_{0.9}Zn_{0.1}Te$ were then extracted from a multiple-sample, multiple-model VASE analysis. The values of both dielectric functions of CZT and its native oxide were fine-tuned in the final fitting process of the analysis.

4.1 Optical properties of CdTe native oxide

VASE measurements were made on a CdTe sample covered with native oxide and analyzed via the assumed surface model shown in Fig. 1. A two-oscillator analytical model with eight parameters [6] was used to describe the dielectric function for native oxide on CdTe. It is expressed as

$$\varepsilon(\hbar\omega) = a + b\hbar\omega - \frac{Ae^{i\phi}}{\hbar\omega - E + i\Gamma}, \tag{4}$$

where A is the amplitude, E is center energy, Γ is the broadening, ϕ is phase in degrees, and $a = a_1 + ia_2$ and $b = b_1 + ib_2$ are complex parameters that allow for a linear background by considering absorption edges at higher energies. It is useful for VASE analysis to separate Eq. 4 into its real and imaginary parts ε_1 and ε_2 as follows

$$\varepsilon_1(\hbar\omega) = a_1 + b_1\hbar\omega + \frac{-A(\hbar\omega - E)\cos\phi - A\Gamma\sin\phi}{(\hbar\omega - E)^2 + \Gamma^2} \tag{5}$$

$$\varepsilon_2(\hbar\omega) = a_2 + b_2\hbar\omega + \frac{-A(\hbar\omega - E)\sin\phi + A\Gamma\cos\phi}{(\hbar\omega - E)^2 + \Gamma^2} \tag{6}$$

The analytical model for native oxide was fit to VASE data acquired on CdTe in the range 0.75 to 6.24 eV, while the optical constants of CdTe substrate were quoted from literature.[7] The results of VASE analysis for CdTe are shown in Fig. 2. The oxide thickness, d_{ox}, for this sample was found to be 52.4 Å. As we can see, a good fit has been achieved for native oxide of CdTe. The optical constants of native oxide (CdTe-ox) of CdTe are shown in Fig. 3 in n and k format. The results shown in Fig. 3 were later used as starting values for $Cd_{0.9}Zn_{0.1}Te$ characterization. Shown in Table 1 are the parameters used to describe CdTe-ox. in Fig. 4.

4.2 Optical dielectric response of $Cd_{0.9}Zn_{0.1}Te$

VASE data acquired on two CZT samples were analyzed using a multiple-sample, multiple-model technique.[8] The two models for this analysis are sketched in Fig. 4. The multiple-sample, multiple-model analysis provides possibilities to remove or reduce the correlation between variables during the fitting process. The optical constants of both CZT substrates in this analysis scheme were coupled together assuming the same values. The oxide overlayer used in Fig. 4 is described by CdTe-ox. We believe it is a reasonable assumption for $Cd_{0.9}Zn_{0.1}Te$ characterization since the 10% Zinc component will not alter the optical properties of the oxide significantly. This assumption was proved to be correct in our final analysis. The oxide thickness of each sample was treated as an independent variable during the fitting. The surface roughness of sample B was modeled using a linearly graded overlayer with effective medium approximation (EMA).[9] The EMA layer was consisted of voids and CdTe-ox. The void fraction varied from 0% at the interface to 50% at the top of the sample surface. The factor of back-surface reflection of sample A (due to both polished surfaces) was also considered in the model. The results of this VASE analysis are shown in Fig. 5. As results, oxide thickness of

sample A, $d_{A\text{-}ox}$, was 43.5Å while that for sample B, $d_{B\text{-}ox}$, was 120.0Å (including surface roughness). In Fig. 5, we can see a good fit has been achieved using this multiple-sample, multiple-model method. We believe the difference between the best fit of ψ and the VASE data in the energy range below 1.5 eV for sample A was due to incomplete removal of the back-surface reflections in the analysis. The extracted dielectric functions of $Cd_{0.9}Zn_{0.1}Te$, $\varepsilon = \varepsilon_1 + i\varepsilon_2$, in a spectral range of 0.75 to 6.24 eV are shown in Fig. 6, in comparison to dielectric functions of CdTe. A wider energy range extending to 6.24 eV has been used here since experimental data were available to that point for one of the CZT samples. In the ε_2 curve the critical points E_1 at ~3.3 eV and $E_1 + \Delta_1$ at ~3.9 eV have been broadened and slightly blue shifted. We believe the broadening is due to the alloy optical scattering from CZT crystal. The blue shift is consistent with the fact of wider band gap of $Cd_{0.9}Zn_{0.1}Te$. A spectroscopic tabulation of the optical constants for $Cd_{0.9}Zn_{0.1}Te$ is provided in Table 2.

A Kramers-Kronig (KK) transformation relation was employed to check the consistency of the dielectric function of $Cd_{0.9}Zn_{0.1}Te$. The KK transformation reflects the nature of relation between the real and imaginary part of the dielectric function $\varepsilon = \varepsilon_1 + i\varepsilon_2$, and can be written as

$$\varepsilon_1(\hbar\omega) = 1 + \frac{2}{\pi} p\int_0^\infty \frac{x\varepsilon_2(x)}{x^2 - (\hbar\omega)^2} dx \qquad (7)$$

where $\hbar\omega$ is the photon energy.[8] By the KK transformation, the real part of the dielectric function ε_1 can be obtained through the imaginary part ε_2. However, the KK transformation integrates the entire spectral range, while our VASE measurements are limited in the range of 0.75-6.24 eV. One non-broadening oscillator was employed to cover the unmeasured spectral range. The modified KK transformation is then written as

$$\varepsilon_1^{KK}(\hbar\omega) = \varepsilon_1^{offset} + \frac{A}{(\hbar\omega)^2 - E^2} + \frac{2}{\pi} p \int_{0.75eV}^{6.24eV} \frac{x\varepsilon_2^{meas}(x)}{x^2 - (\hbar\omega)^2} dx \quad (8)$$

where A and E are the amplitude and center energy for the oscillator, respectively.[8] An ε_1^{offset} was used to replace the unit value in the KK relation. Thus, values of ε_2 obtained through VASE analysis were used to calculate ε_1 via the KK relation Eq. 8. The calculated values were compared with the VASE determined ε_1 values through a regression analysis by varying the values of A, E, and ε_1^{offset} until calculated and measured values match as closely as possible. The results of the KK fit are shown in Fig. 7 and demonstrate that the dielectric response is Kramers-Kronig consistent. A similar KK fit was also performed on the dielectric functions of native oxide of CdTe and $Cd_{0.9}Zn_{0.1}Te$.

A five-Lorentz-oscillator function was utilized to represent the dielectric response for $Cd_{0.9}Zn_{0.1}Te$. It is useful to describe dielectric functions using Lorentz oscillators because they may be expressed as analytical functions. The Lorentz oscillator function is shown in Eq. 9.

$$\varepsilon(E) = \varepsilon_1(\infty) + \sum_{i=1}^{N} \frac{A_i}{E_i^2 - E^2 - i\Gamma_i E} \quad (9)$$

Here, $\varepsilon(E)$ is the complex dielectric function as a function of photon energy, $\varepsilon_1(\infty)$ is the value of the real part of the dielectric function at very large photon energies, and N is the total number of oscillators. Each oscillator is described by three parameters. A_i is the amplitude of the i^{th} oscillator, which has units of $(eV)^2$, Γ_i is the broadening of the i^{th} oscillator, which has units of (eV), and E_i is the center energy (location) of the i^{th} oscillator also in units of (eV).[5,10,11] Fig. 8 shows the dielectric functions, in a range of 1.6 to 6.24 eV, fit from the five-Lorentz-oscillator model, as described above, in comparison to the measured dielectric response of $Cd_{0.9}Zn_{0.1}Te$.

The fit and measured values shown in Fig. 8 overlap almost entirely demonstrating a very good fit by the Lorentz oscillator model. The parameters used in this fit are provided in Table 3. Some values of the critical points of the electron energy band (e.g., E_1 and $E_1 + \Delta_1$) coincide with the center energies of the respective oscillators.

Transmission measurements on both $Cd_{0.9}Zn_{0.1}Te$ and CdTe were performed. The intensity transmission spectra are shown in Fig. 9. It is noticeable that the absorption band edges are 1.46 and 1.58 eV, for CdTe and $Cd_{0.9}Zn_{0.1}Te$, respectively. Those absorption band edges reflect the difference in energy band gaps of CdTe and $Cd_{0.9}Zn_{0.1}Te$ due to the ~10% Zinc forming an alloy of CZT.

5. Conclusions

Optical dielectric functions of $Cd_{0.9}Zn_{0.1}Te$ were determined by VASE measurements in air at room temperature in the range of 0.75 to 6.24 eV, via a multiple-sample, multiple-model analysis. The optical responses of native oxides on CdTe and CZT were also obtained by VASE measurements via a two-Lorentz-oscillator analytical model. The dielectric functions of $Cd_{0.9}Zn_{0.1}Te$ and its native oxides satisfy the Kramers-Kronig relation, respectively. A five-Lorentz-oscillator model was employed to describe the $Cd_{0.9}Zn_{0.1}Te$ dielectric responses analytically, in a range of 1.6 to 6.24 eV. Transmission measurements were performed on both CdTe and $Cd_{0.9}Zn_{0.1}Te$ to demonstrate the different absorption edges at 1.46 and 1.58 eV, respectively.

Acknowledgments

This work was supported by the U.S. Department of Energy, Office of Research and Development within the Office of Nonproliferation and National Security.

References

1. "Semiconductors for Room-Temperature Nuclear Detector Applications," *Semiconductors and Semimetals*, ed. T.E. Schlesinger and R.B. James, Vol. 43 (San Diego: Academic, 1995).
2. H. Yao, J.C. Erickson, L.A. Lim, and R. B. James, *Thin Solid Films*, **313-314**, 351 (1998).
3. R.M.A. Azzam and N.M. Bashara, *Ellipsometry and Polarized Light*, (North-Holland, Amsterdam, 1977).
4. D.E. Aspnes, *Handbook of Optical Constants of Solids*, ed. E.D. Palik, (New York: Academic, 1985), p. 89.
5. H. Yao, P.G. Snyder, and J.A. Woollam, *J. App. Phys.*, **70,** 3261 (1991).
6. S. Zollner, *Appl. Phys. Lett.*, **63**, 2523 (1993).
7. H. Arwin and D.E. Aspnes, *J. Vac. Sci. Technol. A*, **2**, 1316 (1984).
8. H. Yao, B. Johs, and R. B. James, *Phys. Rev. B*, **56**, 9414 (1997).
9. D.E. Aspnes, J.B. Theeten, and F. Hottier, *Phys. Rev. B*, **20**, 3292 (1979).
10. F. Wooten, *Optical Properties of Solids*, (New York: Academic, 1972).
11. M. Erman, J.B. Theeten, P. Chambon, S.M. Kelso, and D.E. Aspnes, *J. Appl. Phys.*, **56**, 2664 (1984).

FIGURE CAPTIONS

1. Sample surface model structure used for VASE analysis for CdTe.
2. Experimental and model best fit from VASE analysis for CdTe. CdTe-oxide was determined to be 52.4Å in the analysis.
3. CdTe-oxide optical constants n and k extracted from the best fit analysis shown in Fig. 2.
4. Sample surface model structures used for VASE analysis for each $Cd_{0.9}Zn_{0.1}Te$ sample. Here the substrate optical constants have been coupled.
5. Experimental and model best fit from VASE analysis for each $Cd_{0.9}Zn_{0.1}Te$ sample. Oxide thicknesses were determined to be 43.5 Å and 120.0 Å for samples A and B, respectively.
6. Dielectric functions of $Cd_{0.9}Zn_{0.1}Te$ determined via the VASE analysis in comparison to that of CdTe quoted from literature.[7]
7. Kramers-Kronig self-consistency check of the dielectric function of $Cd_{0.9}Zn_{0.1}Te$. The ε_1 was calculated and fit from measured ε_2 by Eq. (8). The fitting parameters were determined as 12.015 for A, 8.099 for E and 1.059 for ε_1^{offset}.
8. Lorentz oscillator analytical representation of the dielectric response for $Cd_{0.9}Zn_{0.1}Te$ plotted against the VASE measured dielectric response.
9. Intensity transmission spectra for CdTe and $Cd_{0.9}Zn_{0.1}Te$ demonstrating the absorption band edges of 1.46 and 1.58 eV for CdTe and $Cd_{0.9}Zn_{0.1}Te$, respectively.

Table 1. CdTe-ox Parameters Used in Eq. 5 and 6.

A (eV)	E (eV)	Γ (eV)	ϕ (deg)	a_1	a_2	b_1	b_2
1.0375	5.3905	0.7557	311.1	2.5457	0.06	0.0587	0.05

Table 3. Lorentz Oscillator Parameters for $Cd_{0.9}Zn_{0.1}Te$.

Oscillator N	Amplitude $(eV)^2$ A_I	Broadening (eV) Γ_I	Center Energy (eV) E_i
1	24.59	0.98191	4.9582
2	16.764	0.91679	3.9505
3	7.0685	0.56147	3.3226
4	97.106	5.432	5.6773
5	15.068	0.64173	5.2671

Table 2. Optical Properties for $Cd_{0.9}Zn_{0.1}Te$.

eV	ε_1	ε_2	n	k	α (10^3 cm^{-1})
6.200	-2.362	4.136	1.096	1.888	1185.16
6.100	-2.424	4.387	1.137	1.928	1191.17
6.000	-2.625	4.648	1.165	1.995	1212.46
5.900	-2.954	5.030	1.200	2.096	1252.45
5.800	-3.347	5.616	1.263	2.223	1305.88
5.700	-3.681	6.466	1.371	2.358	1361.29
5.600	-3.834	7.590	1.528	2.484	1408.60
5.500	-3.639	8.914	1.730	2.576	1434.64
5.400	-2.978	10.269	1.964	2.614	1429.74
5.300	-1.840	11.428	2.206	2.590	1390.09
5.200	-0.345	12.161	2.431	2.501	1317.14
5.100	1.257	12.346	2.614	2.361	1219.65
5.000	2.699	12.026	2.741	2.194	1110.89
4.900	3.804	11.375	2.811	2.024	1004.24
4.800	4.524	10.602	2.833	1.871	909.61
4.700	4.913	9.869	2.823	1.748	832.04
4.600	5.068	9.272	2.796	1.658	772.45
4.500	5.080	8.847	2.764	1.600	729.27
4.400	5.024	8.603	2.737	1.571	700.22
4.300	4.957	8.547	2.724	1.569	683.25
4.200	4.957	8.692	2.735	1.589	675.86
4.100	5.156	9.018	2.788	1.617	671.56
4.000	5.702	9.355	2.886	1.621	656.60
3.900	6.528	9.398	2.998	1.568	619.14
3.800	7.281	9.026	3.072	1.469	565.29
3.700	7.679	8.504	3.093	1.375	515.09
3.600	7.802	8.202	3.092	1.326	483.54
3.500	8.017	8.260	3.125	1.322	468.50
3.400	8.690	8.419	3.224	1.306	449.58
3.300	9.768	8.145	3.353	1.215	405.91
3.200	10.720	7.250	3.440	1.054	341.56
3.100	11.151	6.027	3.452	0.873	274.09
3.000	11.070	4.933	3.405	0.724	220.08
2.900	10.772	4.146	3.340	0.621	182.25
2.800	10.458	3.591	3.280	0.547	155.25
2.700	10.181	3.168	3.228	0.491	134.16
2.600	9.936	2.820	3.183	0.443	116.62
2.500	9.713	2.525	3.142	0.402	101.70
2.400	9.509	2.274	3.105	0.366	88.98
2.300	9.324	2.061	3.072	0.335	78.14
2.200	9.160	1.881	3.042	0.309	68.87
2.100	9.022	1.726	3.017	0.286	60.83
2.000	8.913	1.590	2.997	0.265	53.71
1.900	8.836	1.462	2.983	0.245	47.15
1.800	8.795	1.332	2.974	0.224	40.81
1.700	8.803	1.185	2.974	0.199	34.30
1.600	8.966	0.962	2.999	0.160	25.99

Table 2. Optical Properties for $Cd_{0.9}Zn_{0.1}Te$. (continued)

eV	ε_1	ε_2	n	k	α (10^3 cm^{-1})
1.500	8.634	0.150	2.938	0.026	3.88
1.400	8.278	0.025	2.877	0.004	0.62
1.300	8.064	0.012	2.840	0.002	0.28
1.200	7.902	0.000	2.811	0.000	0.00
1.100	7.769	0.000	2.787	0.000	0.00
1.000	7.654	0.000	2.767	0.000	0.00
0.900	7.551	0.000	2.748	0.000	0.00
0.800	7.452	0.000	2.730	0.000	0.00
0.760	7.410	0.000	2.722	0.000	0.00

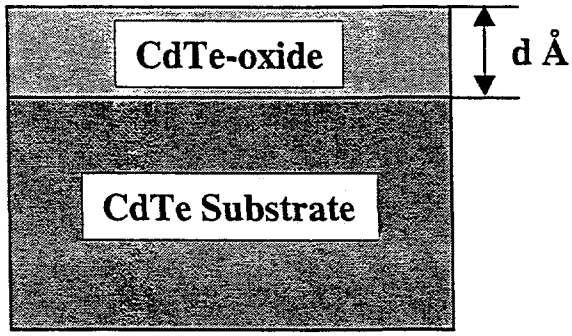
CdTe-oxide
d Å
CdTe Substrate

Fig. 1.

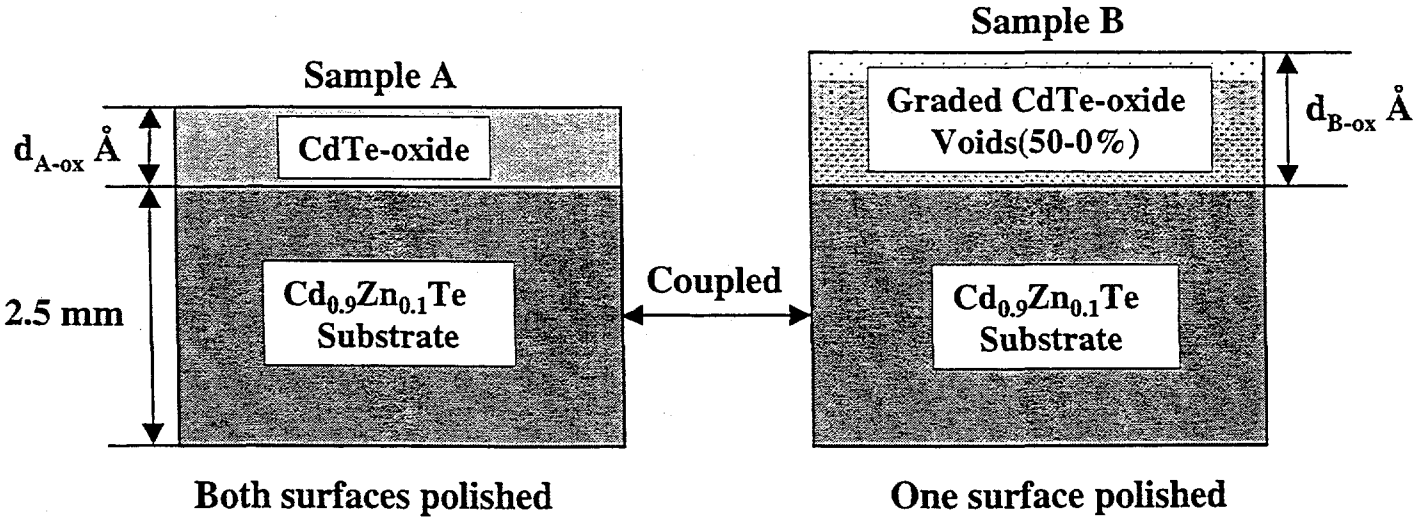
Sample A
Sample B
$d_{A\text{-}ox}$ Å
CdTe-oxide
Graded CdTe-oxide
Voids(50-0%)
$d_{B\text{-}ox}$ Å
2.5 mm
$Cd_{0.9}Zn_{0.1}Te$ Substrate
Coupled
$Cd_{0.9}Zn_{0.1}Te$ Substrate
Both surfaces polished
One surface polished

Fig. 4.

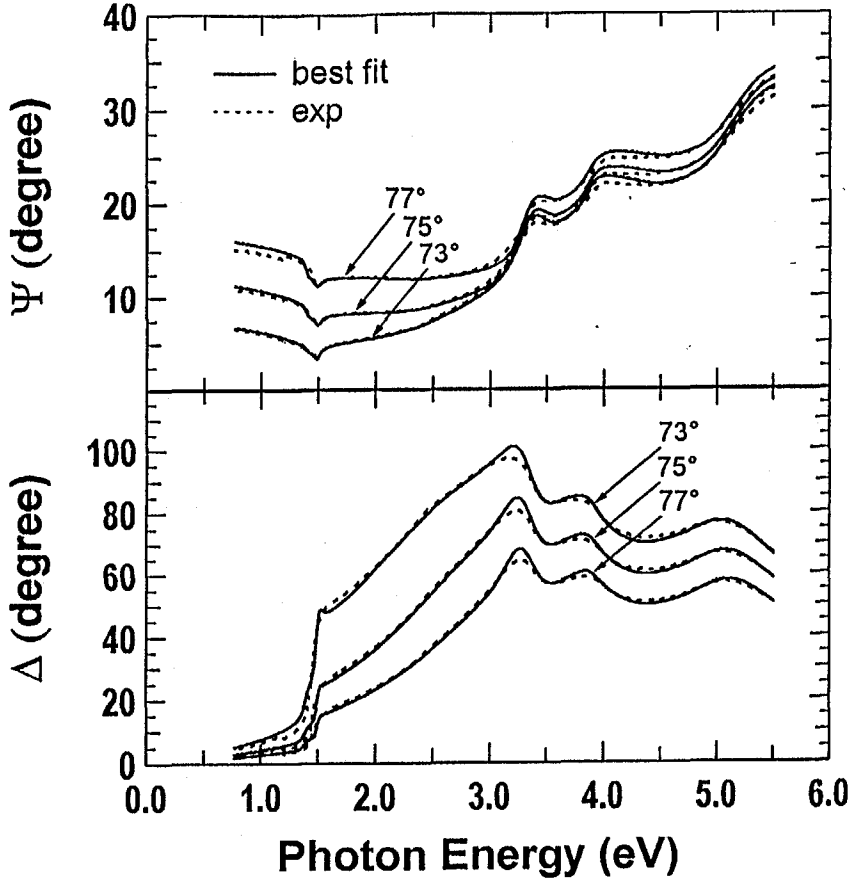
best fit
exp
77°
75°
73°
Ψ (degree)
Δ (degree)
73°
75°
77°
Photon Energy (eV)

Fig. 2.

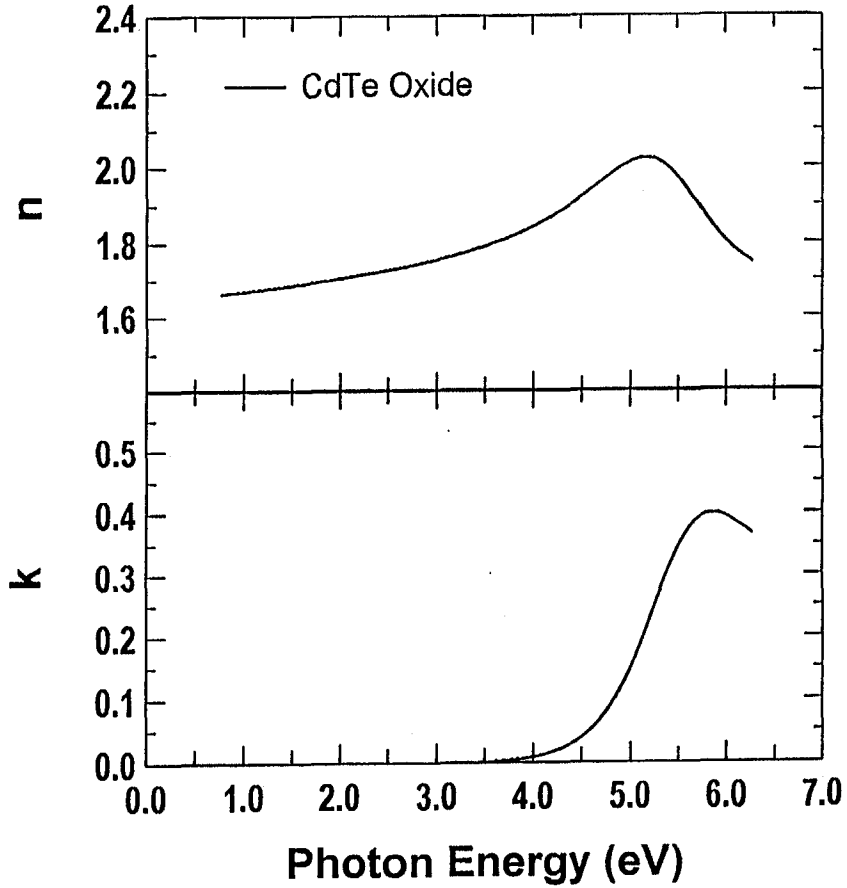
CdTe Oxide
n
k
Photon Energy (eV)

Fig. 3.

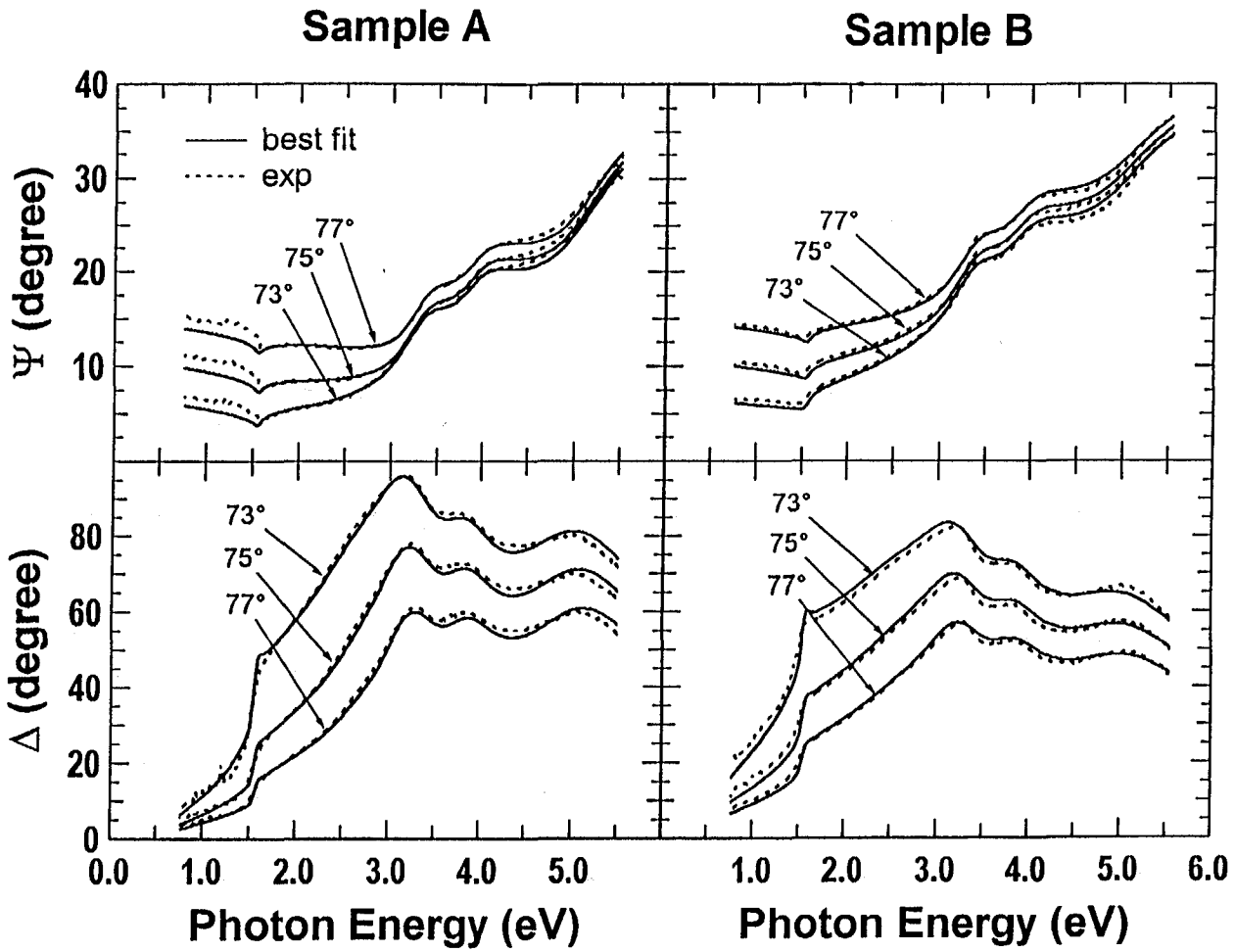
Sample A
Sample B
best fit
exp
77°
75°
73°
Ψ (degree)
Δ (degree)
Photon Energy (eV)
Photon Energy (eV)

Fig. 5.

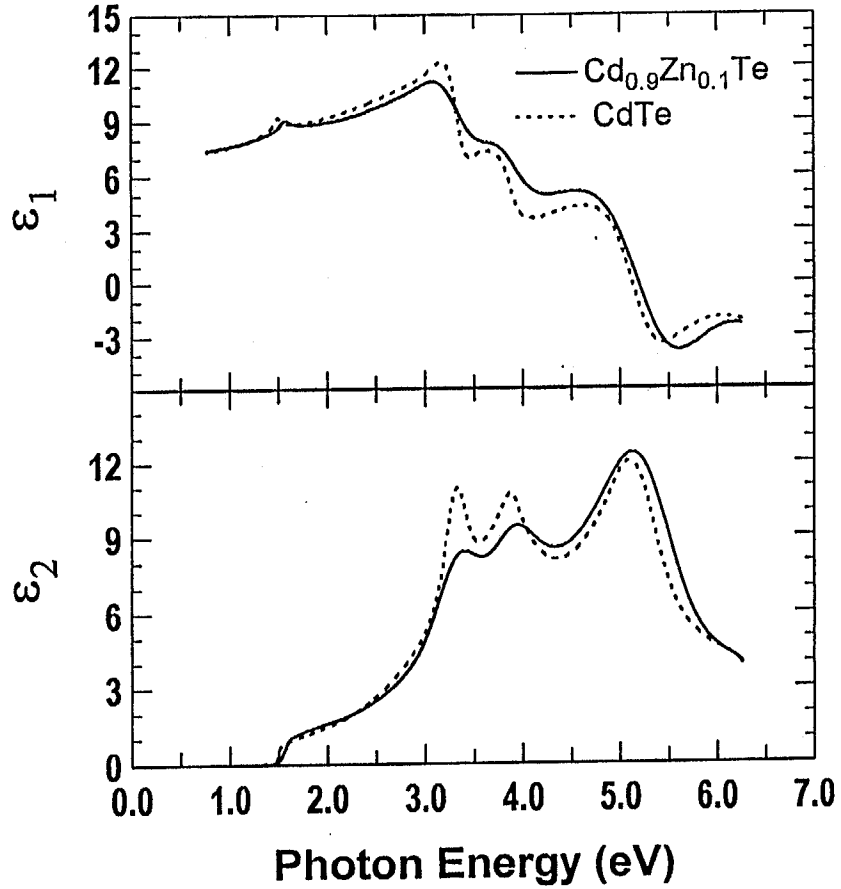
15
12
9
6
3
0
-3
ε_1
$Cd_{0.9}Zn_{0.1}Te$
CdTe
12
9
6
3
0
ε_2
0.0
1.0
2.0
3.0
4.0
5.0
6.0
7.0
Photon Energy (eV)

Fig. 6.

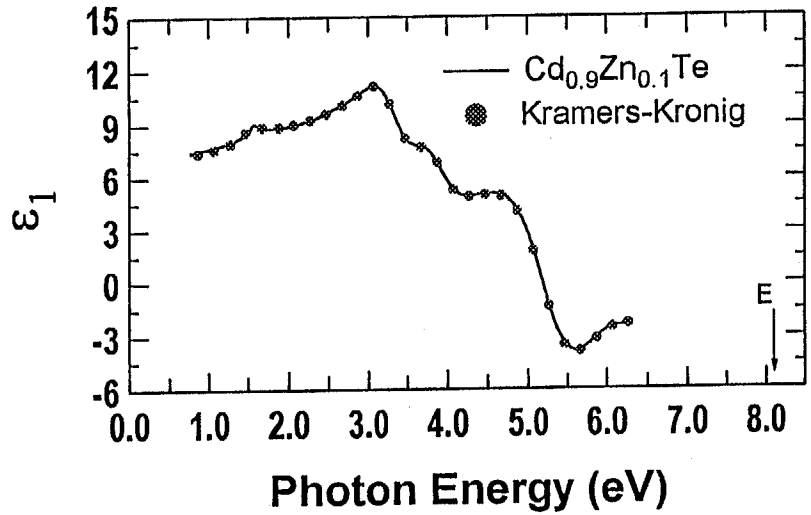
15
12
9
6
3
0
-3
-6
ε_1
$Cd_{0.9}Zn_{0.1}Te$
Kramers-Kronig
E
0.0
1.0
2.0
3.0
4.0
5.0
6.0
7.0
8.0
Photon Energy (eV)

Fig. 7.

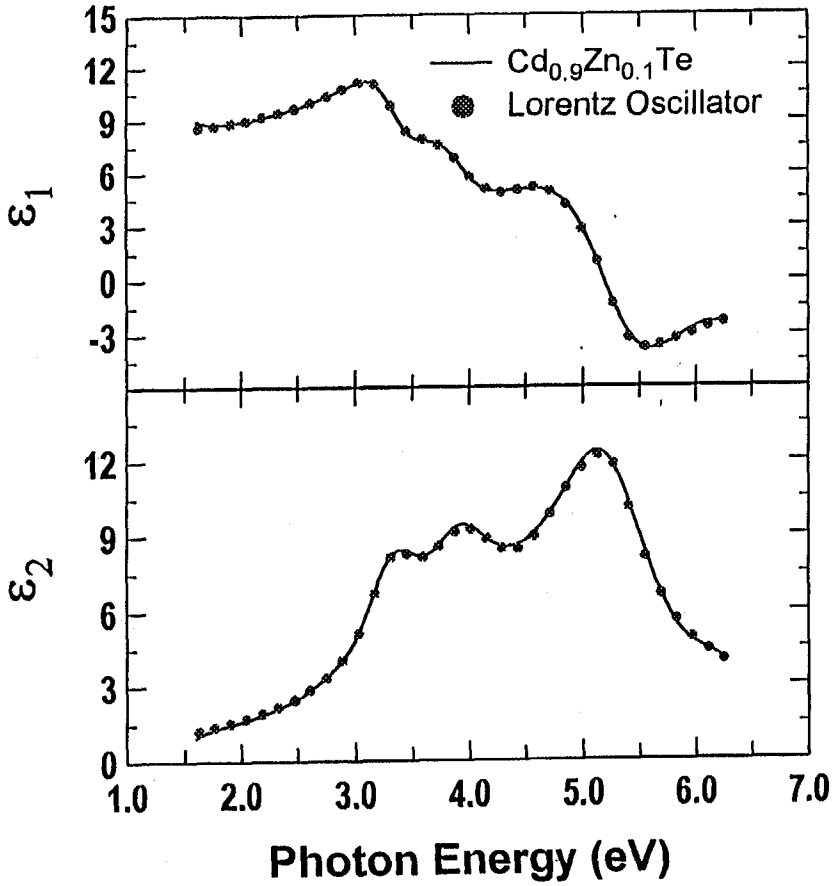
$Cd_{0.9}Zn_{0.1}Te$
Lorentz Oscillator
ε_1
ε_2
15
12
9
6
3
0
-3
1.0
2.0
3.0
4.0
5.0
6.0
7.0
Photon Energy (eV)

Fig. 8.

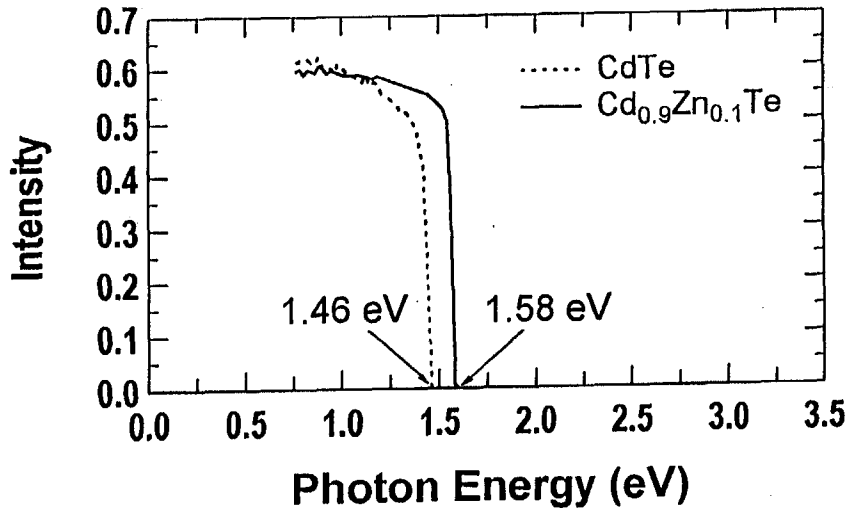
CdTe
$Cd_{0.9}Zn_{0.1}Te$
1.46 eV
1.58 eV
Intensity
0.7
0.6
0.5
0.4
0.3
0.2
0.1
0.0
0.0
0.5
1.0
1.5
2.0
2.5
3.0
3.5
Photon Energy (eV)

Fig. 9.

Multichannel CdZnTe Gamma Ray Spectrometer

F. P. Doty, C. L. Lingren, B. A. Apotovsky, J. Brunsch, J. F. Butler, T. Collins, R. L. Conwell, S. Friesenhahn, J. Gormley, B. Pi, and S. Zhao, Digirad Corporation, San Diego, CA, F. L. Augustine, Augustine Engineering, Encinitas CA., and B. A. Bennett, E. Cross, R. B. James, Sandia National Laboratories, Livermore, CA

Abstract

A 3 cm^3 multichannel gamma spectrometer for DOE applications is under development by Digirad Corporation. The device is based on a position sensitive detector packaged in a compact multi-chip module (MCM) with integrated readout circuitry. The modular, multichannel design will enable identification and quantitative analysis of radionuclides in extended sources, or sources containing low levels of activity. The MCM approach has the advantages that the modules are designed for imaging applications, and the sensitivity can be arbitrarily increased by increasing the number of pixels, i.e. adding modules to the instrument. For a high sensitivity probe, the outputs for each pixel can be corrected for gain and offset variations, and summed digitally. Single pixel results obtained with discrete low noise readout indicate energy resolution of 3 keV can be approached with currently available CdZnTe. The energy resolution demonstrated to date with MCMs for 511 keV gamma rays is 10 keV.

Introduction

Nondestructive analysis of containerized mixed low-level waste (MLLW) and mixed transuranic (MTRU) waste is an important need for DOE. MLLW is defined as waste that contains both hazardous chemical constituents, and radioactive constituents with concentrations below 100 nCi / gram. The characteristics of all mixed waste streams must be adequately documented to satisfy regulatory requirements, and to verify they meet the waste acceptance criteria for specific treatment and disposal facilities. Traditional approaches to characterizing waste streams can be loosely divided into (1) process knowledge, (2) waste sampling and subsequent measurement in analytical laboratories, and (3) non-invasive assay.

Knowledge of the materials and processes that generated a mixed waste can be sufficient for characterization if appropriate records are available, but DOE has insufficient process knowledge to adequately judge the contents of waste containers for 40% of the 130,000 m^3 of LLMW currently in storage[1]. Traditional waste sampling and laboratory analysis can also be used to effectively characterize waste, but the value of obtaining additional analytical data must be carefully evaluated versus exposing workers to measurable radiological dose and chemical hazards during sample collection and subsequent handling. High costs are incurred with mixed waste analysis, because of the need to provide protection and controls that keep radiological exposures as low as reasonable achievable (ALARA). Therefore a critical need exists for a field compatible, high sensitivity detector capable of *in-situ* analysis of radioisotopes in containerized MMLW and MTRU.

Approach

Field compatibility implies low power, portable and non-cryogenic. Energy resolution is also required, to identify specific radionuclides and infer their concentrations. These requirements rule out available detectors such as HPGe, which require cooling, and scintillator-based systems, which have poor energy resolution. One approach is to develop new detectors based on a wide bandgap semiconductor material, such as CdZnTe. The sensitive areas and volumes of CdZnTe and other room-temperature semiconductors are currently limited by material properties[2,3,4,5,6]. The reduced trapping-lengths compared to cooled silicon and germanium devices limit the useful thickness of CZT detectors, while leakage current and capacitance determine the energy resolution of a single-channel large area device. These factors can be mitigated by electron sensitive, multi-anode detectors read out with multiple electronic channels[7,8].

Results from detectors based on the semiconductor CdZnTe (CZT) are reported in this work. CZT detectors, which operate at room-temperature and exhibit improved energy resolution compared to scintillators, are under development by Digirad primarily for medical applications [9,10,11,12]. The approach described here uses 64 element CZT arrays with, with element size 3mm x 3mm x 5mm, read out with an

application specific integrated circuit (ASIC) with separate charge amplification per channel. The ASIC used in this study was designed for imaging rather than spectroscopy, and non-optimal results were obtained. Likewise, the CZT arrays were not selected for spectroscopic resolution or uniformity, and should be perceived as neither representative nor exceptional examples of Digirad's detectors. Rather, the aim of this work is to demonstrate the usefulness of the approach using readily available materials and apparatus.

Spectroscopy with electron sensitive detectors

The detectors employed in Digirad's imaging array modules are of a patented electron-sensitive design which has been described elsewhere[13,14,8]. Electron sensing detectors reduce the dependence of pulse height on the position of photoelectric absorption in the semiconductor (charge-deficit tailing), because electron trapping lengths are usually much greater than hole trapping lengths in current commercially available material. For example, typical electron $\mu\tau$ products are on the order of 10^{-3} cm^2 v^{-1}, which correspond to trapping lengths on the order of 1 cm under practical applied fields. Hole $\mu\tau$ products are typically on the order of 10^{-5} cm^2 V^{-1} or less, with correspondingly reduced trapping lengths. In simple slab geometry detectors of practical dimensions trapped holes result in a reduction in signal, even though electron collection is nearly complete. Therefore, electron sensitive detector designs enable both increased drift length and improved energy resolution.

A spectrum recently obtained with a discrete Digirad SpectrumPlus™ 3mm x 3mm x 5mm production detector element is shown in Figure 1. The resolution of the 511 keV photopeak gamma rays detected from ^{22}Na is >3keV. This result was obtained without cooling any part of the system, using an Oxford/Tenelec TC170 preamplifier, Ortec 672 amplifier/shaper, Oxford PCA3 MCA and Oxford Quantum MCA software. The performance achievable with CZT arrays can approach that of a single discrete element. In principle, the data from multiple calibrated channels with this performance can be digitized, adjusted for response variations and summed, to obtain similar energy resolution with much higher sensitivity.

Spectroscopy with arrays

To date, increased sensitivity has been demonstrated only for CdZnTe arrays with ASIC readouts designed for imaging rather than spectroscopy. Calibration requires accurate determination of the gain for each detector/readout channel. This is easily accomplished by exposing arrays to a flood source, to obtain a large number of counts in each pixel. Results of such an experiment are histogrammed in figures 2 and 3. A 64 element, 25mm x 25mm x 5mm array, read out with a proprietary Digirad ASIC, was irradiated with a 17 μCi ^{57}Co point source located a distance of 5 cm from the center. Data were recorded until the highest channel reached about 10^6 counts, approximately 20 hours.

Figure 2 is a histogram of the total counts per working pixel. The mean number of total counts in the spectra was 1.23×10^7, and the observed standard deviation was 3.55%. The estimated deviation from the detector-source geometry is less than 0.5%, and the statistical deviation between channels with this number of counts should be approximately 0.03%. The remaining variation is mainly attributable to the CdZnTe detector and material properties. Therefore the estimated relative counting efficiency is uniform within about +/- 3% for this particular array.

Figure 3 is a histogram of peak channel numbers for this experiment. The gaps in the histogram indicate a slight differential nonlinearity in the ADC used for this experiment. The approximately gaussian distribution of gains is centered on MCA channel 147, with a standard deviation of 3.4 channels or 2.3%. Thus a slight correction for gain differences is necessary to minimize the peak widths, when summing the data to record a composite spectrum.

The best performance obtained to date using this method is demonstrated in figure 4. The spectrum is a summed composite of gain-corrected spectra from all 64 pixels in a MCM acquired with the isotope ^{22}Na. Note that Digirad's current readout ASIC is designed for low energy applications, thus the gamma ray at 1.27 MeV is not recorded in this demonstration. The energy resolution seen here for the 511 keV line is 10.1 keV. This is only slightly greater than the resolutions expected of the individual channels for this device, and shows that the gain calibration method was successful.

Sources of response variation

The energy resolution achievable with the multichannel approach is determined by the resolution of the individual channels. By calibrating the pulse height data from each channel, the variations indicated in the histogram in figure 3 can be correcting, minimizing the peak widths for composite spectra. The nonuniform response of the individual channels is due to effects in the semiconductor as well as the electronic channels. Therefore this approach somewhat relaxes requirements for semiconductor homogeneity. That is, the material properties must only be uniform on the scale of the pixellation, rather than the entire device, to obtain narrow composite pulse height distributions.

Component tolerances affect the gain distributions by introducing systematic error in each electronic channel. The most important sources of these gain variation in the ASIC are capacitor tolerances and MOSFET bias sensitivity. These effects, and variations in stray capacitance are mainly responsible for the observed 2.3% deviation of the relative gains.

Materials factors can also affect gains, through variations in the CdZnTe alloy composition, trap densities, etc. The compositional variation, which is necessarily present due to segregation in melt-grown crystals, results in variation of the bandgap, and hence the ionization energy of the material. The magnitude of this effect actually depends on the length of the ingot and the position from which a detector is drawn. For 10 kg ingots routinely produced by Digirad the bandgap changes less than 1% per cm over most of the ingot, therefore gain and counting rate variations due to this effect are negligible for individual detectors and monolithic arrays. It is possible, however, for two detectors drawn from different locations to have significant differences in the bandgap. More important materials factors include electron $\mu\tau$ product variations, gross defects and boundary effects. These introduce random error in the pulse heights recorded within individual channels, broadening the pulse height distributions.

Conclusions

An approach to making a field portable, high sensitivity gamma ray spectrometer has been demonstrated. Results were obtained from 25mm x 25mm x 5mm CdZnTe detector array, a sensitive volume of 3 cm^3.

Energy resolution of 10 keV was achieved using non optimal detector material and readout ASIC. Results with a single discrete element and low-noise electronics showed energy resolution > 3 keV is achievable with currently available CdZnTe. To approach this level of performance with a multichannel device will require a new ASIC designed specifically for spectroscopy.

Figures

Figure 1 Spectrum from ^{22}Na obtained with a discrete CZT detector and readout. The resolution is >3keV FWHM for the 511 keV annihilation peak.

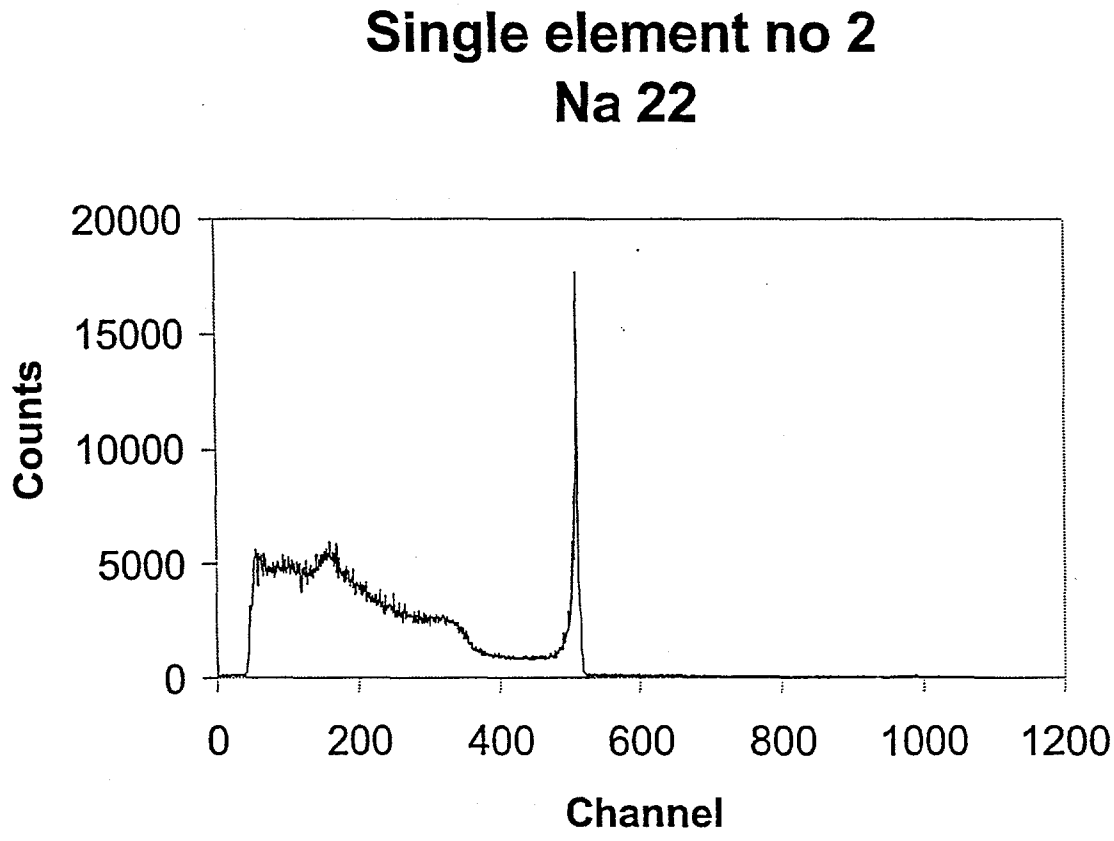

Figure 2 Histogram of ^{57}Co peak channel for a 64 element CZT array. The standard deviation of observed gains is 2.3 %, caused by component tolerances and CZT properties.

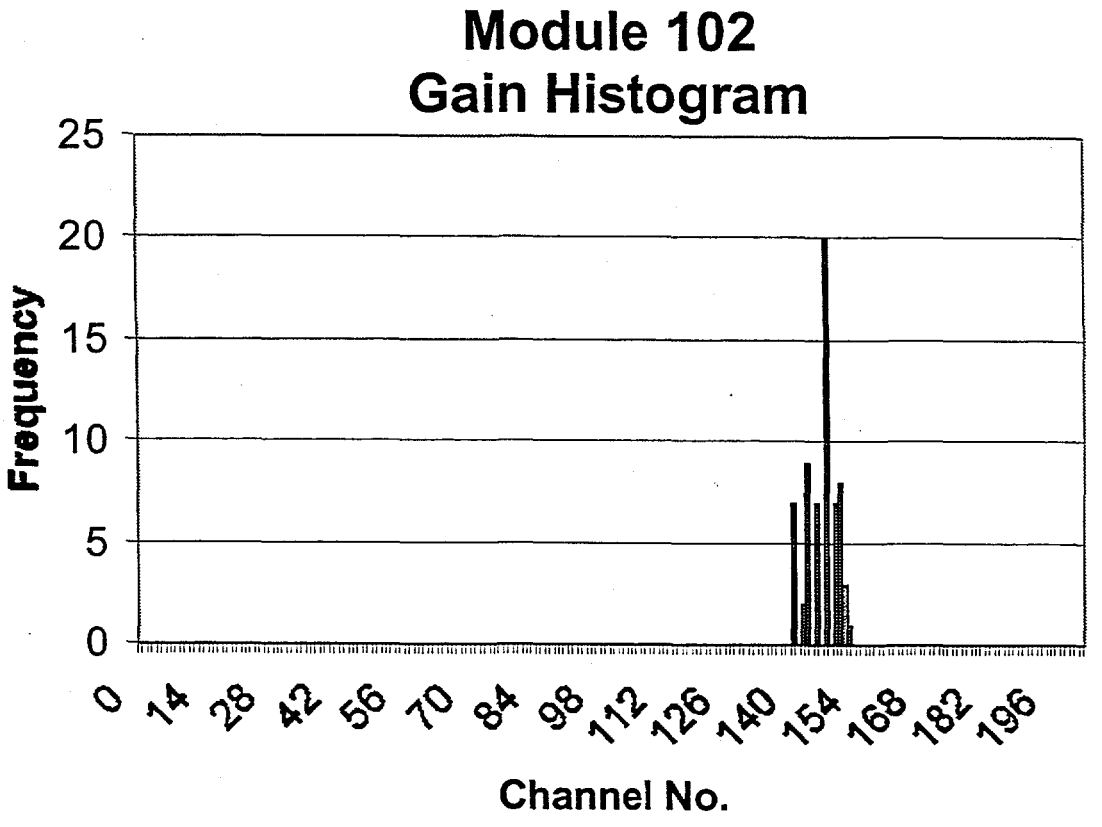

Figure 3 Count rate histogram for the same CZT module as Figure 2. Observed standard deviation of 3.55 % is largely attributable to nonuniform properties of the CZT.

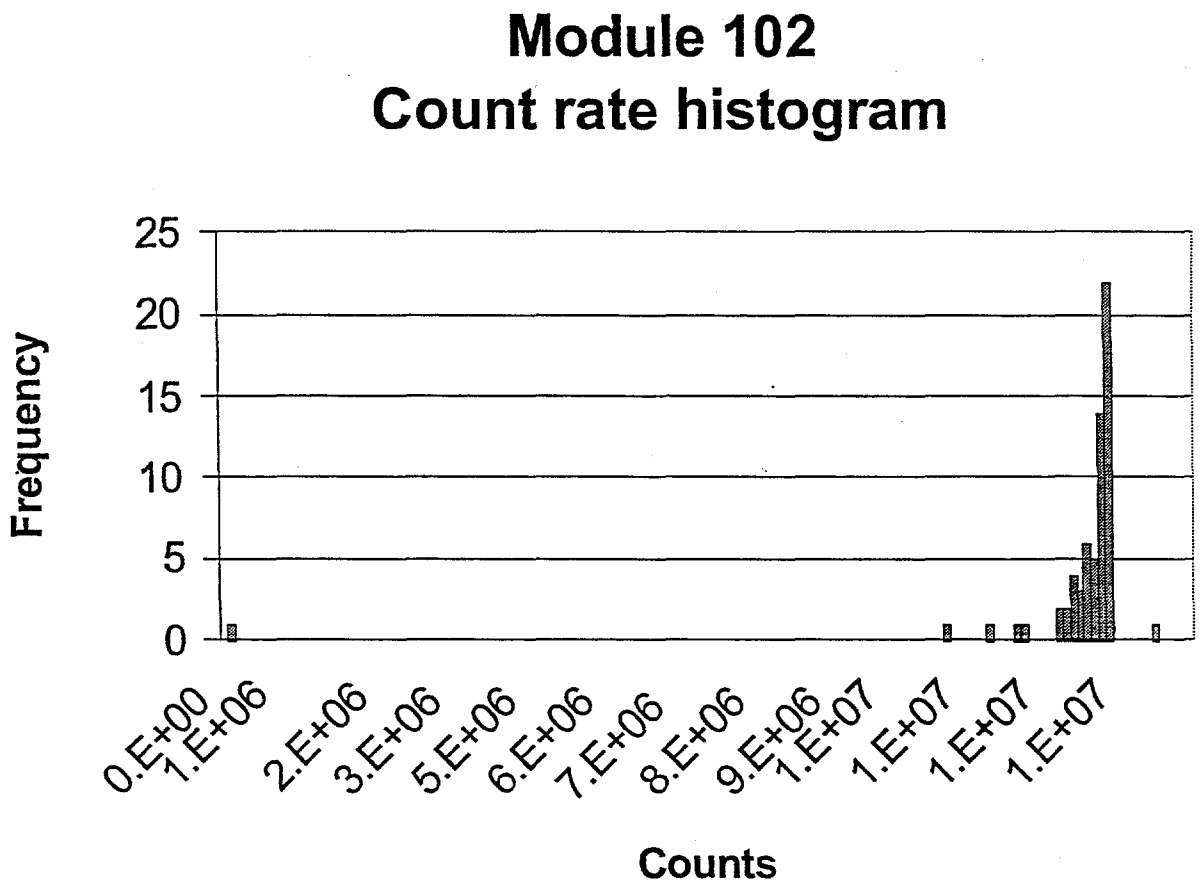

Figure 4 Composite spectrum from ^{22}Na obtained with a 64 element CZT array with ASIC readout. The resolution is 10.1 keV FWHM for the 511 keV annihilation peak Sensitive volume is 25 mm x 25 mm x 5 mm.

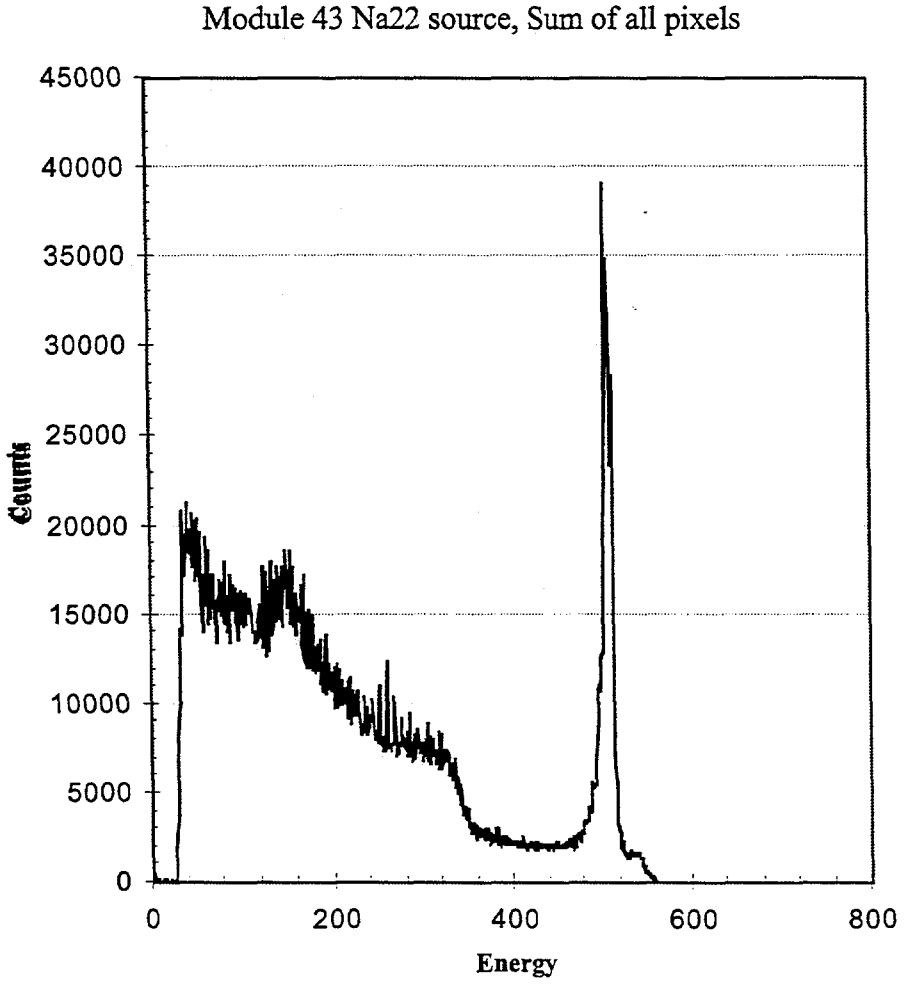

References

1 'Proposed Site Treatment Plans National Summary--National Summary of Mixed Wastes and Treatment Options, DOE EM-30, 1995

2 Semiconductors for room-temperature nuclear detector applications, Semiconductors and Semimetals vol. 43, T. E. Schlesinger and R. B. James (Ed.s), Academic Press, (1995).

3 "Properties of CdZnTe crystals grown by a high pressure Bridgman method", F. P. Doty, J. F. Butler, J. Schetzina, K. Bowers, Proc. 1991 U. S. Workshop on the Physics and Chemistry of HgCdTe and Other II-VI Compounds, D. E. Seiler (Ed.), Journal of Vacuum Science and Technology B10,1418 (1992).

4 "Gamma- and x-ray detectors manufactured from Cd1-xZnxTe grown by a high pressure Bridgman method" J. F. Butler, F. P. Doty, B. A. Apotovsky, Mat. Sci. and Eng. B16,291 (1993).

5 "Charge carrier mobilities in Cd.8Zn.2Te single crystals used as nuclear radiation detectors", Z. Burshtein, H. N. Jayatirtha, A. Burger, J. F. Butler, B. Apotovsky, F. P. Doty, Appl. Phys. Lett. 63,102 (1993).

6 "Carrier mobilities and lifetimes in CdTe and CdZnTe", F. P. Doty, in Properties of Narrow Gap Cadmium-based Compounds, P. Capper (Ed), Electronic Materials Information Service DataReviews Series, 10,540 (1994).

7 "Pixellated Cd1-xZnxTe detector arrays", F. P. Doty, H. B. Barber, F. L. Augustine, J. F. Butler, B. A. Apotovsky, E. T. Young, W. Hamilton, Nuclear Instruments and Methods in Physics Research A 353,356 (1994).

8 Achieving Good Energy Resolution with High Sensitivity in Room-Temperature Gamma-ray Detectors C.L. Lingren, S.J. Friesenhahn, J.F. Butler, Bo Pi, B. Apotovsky, T.C. Collins, F.P. Doty. Nuclear Science Symposium, Albuquerque NM Nov. 1997.

9 "Semiconductor pixel detectors for gamma imaging in nuclear medicine", H. B. Barber, B. A. Apotovski, F. L. Augustine, H. H. Barrett, E. L. Dereniak, F. P. Doty, J. D. Eskin, W. J. Hamilton, D. G. Marks, K. J. Matherson, J. E. Venzon, J. M. Wolfenden and E. T. Young, accepted for Nuclear Instruments and Methods

10 "Progress in developing focal-plane-multiplexer readout for large CdZnTe arrays for nuclear medicine", H. B. Barber, B. A. Apotovsky, F. L. Augustine, H. H. Barrett, E. L. Dereniak, F. P. Doty, J. Eskin, W. Hamilton, K. J. Matherson, D. C. Marks, J. E. Venzon, J. M. Woolfenden, E. T. Young, Nucl. Instrum. Meth. in Phys. Res., A380:262-265, 1996

11 "Semiconductor Gamma-Ray Camera and Medical Imaging System", International Patent No. WO 96/20412 (1996).

12 "X-ray and gamma ray imaging with monolithic CdZnTe arrays", F. P. Doty and P. L. Hink, Proc. SPIE 1945,145 (1993).

13 "Semiconductor Radiation Detector with Enhanced Charge Collection", U.S. Patent No. 5,677,539 (1997).

14 "Semiconductor Radiation Detector with Enhanced Charge Collection", International Patent No. WO 97/14060 (1997).